Reconfigurable Photovoltaic Array Systems for Adaptive and Fault-Tolerant Energy Harvesting

Naehyuck Chang, Massoud Pedram, Hyung Gyu Lee, Yanzhi Wang and Younghyun Kim

Abstract This chapter introduces a reconfigurable photovoltaic (PV) cell array for adaptive and fault-tolerant energy harvesting in view of component modeling, architectures, properties, and reconfigurable algorithms for partial shading and fault tolerance. On top of traditional PV cell array-based energy harvesting research, the dynamically reconfigurable PV cell array gives additional significant benefits in both efficiency and cost. This is a representative example of how electronics design automation contributes to various problems in other domains.

Keywords Photovoltaic system · Solar cell · Reconfiguration · Efficiency · Fault tolerance

N. Chang (✉)
Korea Advanced Institute of Science and Technology, Daejeon, Korea
e-mail: naehyuck@kaist.ac.kr

M. Pedram · Y. Wang
University of Southern California, Los Angeles, CA, USA
e-mail: pedram@usc.edu

Y. Wang
e-mail: yanzhiwa@usc.edu

H.G. Lee
Daegu University, Daegu, South Korea
e-mail: hglee@daegu.ac.kr

Y. Kim
Purdue University, West Lafayette, IN, USA
e-mail: yhkim1@purdue.edu

C.-M. Kyung (ed.), *Nano Devices and Circuit Techniques for Low-Energy Applications and Energy Harvesting*, KAIST Research Series,
DOI 10.1007/978-94-017-9990-4_6

1 Introduction

Due to increasing demand for energy sources and environmental concerns about fossil fuels as well as self-sustainable and maintenance-free operations, there has been a growing demand for energy harvesting power supply systems. There are ranges of energy harvesting sources from microwatt to megawatt or higher power capacity applications. Photovoltaic (PV) energy generation has received significant attention due to relatively higher energy density from milliwatts to megawatts among various energy harvesting power sources. The PV cell efficiency ranges from 20 to 30 % in commercial products and exhibits even a higher efficiency in the lab. PV cell power generation is largely affected by environmental factors such as time of day, season, weather, etc. However, short-term PV cell power generation stability is superior to other renewable power sources such as windmills. PV power generation does not require moving parts subject to wear and tear, noise, and vibration, etc., which is crucial for portable and long-term applications. This chapter focuses on PV power generation for small power applications below a kW order.

Thanks to extensive research efforts on PV power generation technologies, various scales of PV systems have been deployed for practical applications, such as PV power stations, solar-powered vehicles, and solar power heating and lighting appliances. This chapter presents the power models of PV energy harvesting system subcomponents, maximum power point tracking (MPPT), and maximum power transfer tracking (MPTT), reconfigurable PV cell arrays for partial shading and fault tolerance. This chapter also introduces a light-weight PV energy harvesting system that does not require power converters or energy storage elements while it performs MPPT.

1.1 Structure of PV Energy Harvesting Systems

The PV energy harvesting systems are comprised of a PV cell array, a load device, and a power converter between the PV cell array and the load device. There is an optional energy storage element between the PV cell array and the load device, and a power converter between the energy storage element and load device. Figure 1 illustrates two simplified PV energy harvesting system examples. Figure 1a does not include an energy storage element, and thus the load device is directly powered by the PV cell. There is a power converter between the PV cell array and the load device because it is generally hard to match the PV cell array output voltage with the load device supply voltage. Assuming that load device current is independent of the solar irradiance and temperature, which is a typical situation, the PV cell array output current is independent of the solar irradiance and temperature accordingly. It is crucial to control the PV cell array output current so that the PV cells output power is maximized. This is the so-called MPPT, which is

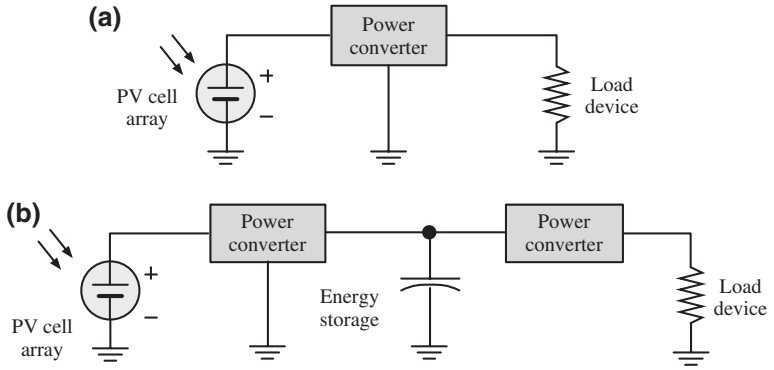

Fig. 1 Simplified diagrams of PV energy harvesting systems. **a** A PV energy harvesting system without an energy storage. **b** A PV energy harvesting system with an energy storage

explained in Sect. 2.3.1. To make a long story short, it is hard to realize the MPTT with the setup of Fig. 1a due to the mismatch between the load current and the maximum power point (MPP) PV cell array current. This chapter introduces a new MPTT with the architecture of Fig. 1a in Sect. 4.

In order to maintain the operating point at the MPP regardless the load current, we commonly use the architecture in Fig. 1b for the MPTT of the PV cell array though the load device does not have to operate when there is no solar irradiance. The energy storage element in Fig. 1b is, of course, useful to make the PV energy harvesting system functional even if there is solar irradiance interruption. Most energy storage elements exhibit variable terminal voltage by the state of charge and the load current. The nominal voltage of batteries is determined by the battery chemistry, and the terminal voltage of a capacitor is a linear function of the state of charge, which does not match with the load device power supply voltage in general. Therefore, there should be another power converter between the energy storage element and load device.

The power converter between the PV cell array and energy storage element keeps tracking of the PV cell array MPP current. In other words, the charging current to the energy storage element is not constant at all times unlike a battery charger plugged into the wall. The charging current keeps track of the MPP current of the PV cell array around the clock. We call this power converter an *MPP charger*. The power converter between the energy storage element and the load device is commonly a voltage regulator. We prefer to use switching-mode DC-DC converters both for the MPP charger and the voltage regulator for high conversion efficiency. Section 2.2 covers power efficiency and models of switching-mode DC-DC converters.

The energy storage element should provide a desired nominal voltage, nominal capacitance, minimum cycle efficiency, minimum cycle life, energy density, power density, form factor, cost, etc. Rechargeable batteries are commonly used considering these requirements. Lithium-ion batteries are preferred for high-performance

systems, and lead-acid batteries are considered for cost-efficient systems. One of the primary design goals of PV energy harvesting systems is low maintenance cost. The batteries in the PV energy harvesting systems become a primary cause of the limited lifetime. Electric double-layer capacitors (supercapacitors) are promising replacements of rechargeable batteries, thanks to their virtually unlimited cycle life. There are distinct shortcomings of supercapacitors, but their advantages often override their drawbacks in particular applications.

1.2 Design Consideration and Runtime Management

A PV cell is a semiconductor device that produces relatively low open-circuit and MPP voltages. The MPP current is a function of the PV cell area, and there are cost-effective sizes of the PV cell for mass production. Aside from a very small, low-power applications, the load device supply voltage and current are generally higher than a PV cell MPP voltage and current. This makes the PV energy harvesting systems use an array of PV cells instead of a single PV cell. The power converter, MPP charger, is connected to both ends of the PV cell array, which is named as a string inverter (converter) architecture. The string inverter architecture is cost effective but subject to degradation due to partial shading. This chapter gives a closer look into the partial shading problem and provides novel online PV cell array reconfiguration; a PV energy harvesting system, a typical example that requires a *cross-layer optimization*. The dynamically reconfigurable PV cell array must come with a novel management algorithm to maintain its maximum efficiency. Section 3 introduces a dynamically reconfigurable PV cell array architecture and algorithms to combat partial shading and temperature variation. This section also covers fault-tolerant features of the PV cell array.

Power converters are the primary factor of efficiency degradation. The energy storage element is subject to efficiency loss as well. Batteries' cycle efficiency and limited rate capability result in significant power loss. Supercapacitors show a very high cycle efficiency, but their severe terminal voltage variation by the state of charge makes it difficult for the power converters to maintain a high efficiency. Most of all, the power converters and energy storage elements are bulky, heavy, and expensive, which seriously discourage to implement low cost, tiny energy harvesting systems. Section 4 introduces a breakthrough MPPT method without the power converters and energy storage element for low-power PV energy harvesting applications.

The architecture in Fig. 1a does not give a freedom in the charge management of PV energy harvesting systems. The PV cell array harvests solar energy, and the load device uses the harvested energy immediately. However, Fig. 1b has an energy storage element, and thus energy harvesting and consumption can be independent of each other. In other words, energy harvesting can be done following the MPPT, and the load device energy consumption can be determined by its workload (user demand) and the power management policy. The average power coming into the

energy storage element should not be smaller than the power coming out from it at all times to avoid service interruption. Determination of the energy storage element is typically constrained by its minimum capacity when it comes to the battery-based energy storage. A larger size of the battery shows better cycle efficiency due to lower internal impedance and higher rate capability, a longer cycle life due to less number of cycles, but its cost, volume, and weight increase. On the other hand, a supercapacitor-based energy storage makes the design consideration more complicated. Section 2.3.2 introduces a new concept of MPPT, called MPTT, that jointly optimizes the power efficiency of the PV cell array and the power converter.

2 Efficiency of Photovoltaic Cell Energy Harvesting Systems

In this section, we first present a PV cell power model and a switching converter power model, which are two dominant components to the overall energy efficiency of solar energy harvesting systems. Next, we discuss and compare two operational techniques to maximize the output power of PV cells. Lastly, we discuss how the partial degradation of a PV cell array due to shading or permanent fault affects the performance of the array.

2.1 PV Cell Modeling

The basic building block of a PV array is a PV cell. The PV cells exhibit highly nonlinear voltage-current (V-I) output characteristics (curves) that change with the solar irradiance level. Figure 2a shows the PV cell V-I output characteristics

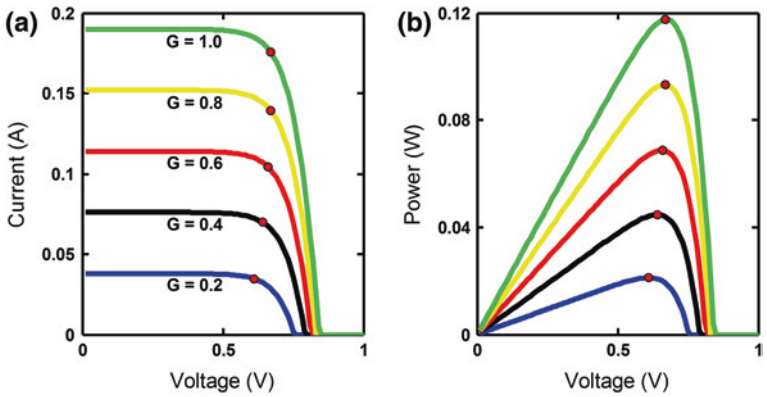

Fig. 2 V-I and V-P output characteristics of a PV cell and MPPs

under different solar irradiance levels. Figure 2b shows the corresponding voltage-power (V-P) output characteristics. The red dots in Fig. 2 denote the maximum power points (MPPs) of a PV cell where the PV cell achieves the maximum output power for the given solar irradiance level. Notations used in this section are listed in Table 1.

Let V^{pvc} and I^{pvc} denote the output voltage and current of a PV cell, respectively. The PV cell equivalent circuit model is shown in Fig. 3 with the V-I output characteristics given by

$$I^{\text{pvc}} = I_L - I_d - I_{\text{sh}} = I_L(G) - I_0(T) \cdot (e^{(V^{\text{pvc}} + I^{\text{pvc}} \cdot R_s) \cdot \frac{q}{AkT}} - 1) - \frac{V^{\text{pvc}} + I^{\text{pvc}} \cdot R_s}{R_p} \tag{1}$$

where

$$I_L(G) = \frac{G}{G_{\text{STC}}} \cdot I_L(G_{\text{STC}}) \tag{2}$$

and

$$I_0(T) = I_0(T_{\text{STC}}) \cdot (\frac{T}{T_{\text{STC}}})^3 \cdot e^{\frac{qE_g}{Ak} \cdot (\frac{1}{T_{\text{STC}}} - \frac{1}{T})} \tag{3}$$

Parameters in (1)–(3) are defined as follows: G is the solar irradiance level; T is the cell temperature; q is the charge of the electron; E_g is the energy bandgap; and k is the Boltzmann's constant. STC stands for standard test condition in which the irradiance level is 1000 W/m^2 and the cell temperature is 25 °C. The parameters listed above are either physical constants, environment-related value or

Table 1 Notations used in Sect. 2.1

V^{pvc}	Output voltage of a PV cell
I^{pvc}	Output current of a PV cell
$I_L(G)$	The photo-generated current at solar irradiance G
$I_0(T)$	Dark saturation current at temperature T
R_s	PV cell series resistance
R_p	PV cell parallel resistance
A	The diode ideality factor
q	Charge of an electron
E_g	The energy bandgap

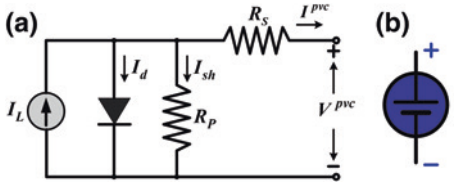

Fig. 3 Electronic circuit equivalent model (**a**) and symbol (**b**) of a PV cell (Reproduced with permission from Wang et al. [22])

configuration parameters. There are still five unknown parameters, commonly not provided by manufacturers, to be determined. These five parameters are the key that is capable of analytically describing the characteristics of a PV cell:

- $I_L(G_{\mathrm{STC}})$: the photo-generated current at standard test condition.
- $I_0(T_{\mathrm{STC}})$: dark saturation current at standard test condition.
- R_s: PV cell series resistance.
- R_p: PV cell parallel (shunt) resistance.
- A: the diode ideality factor.

We extract the unknown parameters from measured PV cell V-I curves at various irradiance levels and temperatures, in which each V-I curve is measured using data acquisition equipment under one specific environmental condition (G, T). Therefore, our parameter extraction method is not confined to only the parameters at STC. Instead, it extracts $I_L(G_0)$ and $I_0(T_0)$ flexibly under any environmental condition (G_0, T_0) from the measured data. Subsequently, the corresponding parameters at STC, $I_L(G_{\mathrm{STC}})$ and $I_0(T_{\mathrm{STC}})$, can be determined using (2) and (3). We apply the proposed combined parameter extraction method on the measured PV cell V-I curves [1]. Significant reduction (on average 8X) in root mean square (RMS) fitting error can be observed compared with the conventional method which only considers some specific points.

2.2 Power Converter (Charger) Power Model

Figure 4 shows the model of a PWM (pulse width modulation) buck-boost switching converter, which is used as the charger in the proposed PV system. The input ports of the charger are connected to the PV panel/array, whereas the output ports are connected to the EES element. The charger regulates the operating point of the PV panel by controlling the charger's input voltage, i.e., the PV output voltage (and then the PV panel output current is automatically determined by its V-I characteristics.) Notations used in this section are listed in Table 2. We denote the input voltage, input current, output voltage, and output current of the charger by V_{in}, I_{in}, V_{out}, and I_{out}, respectively. Depending on the relationship between V_{in} and

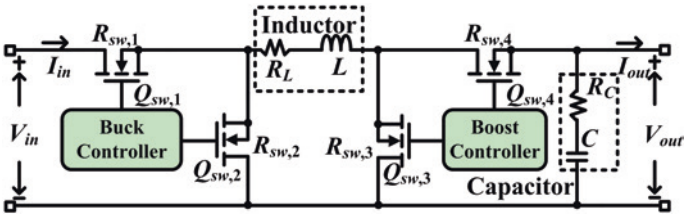

Fig. 4 Power converter electronic modeling (Reproduced with permission from Wang et al. [22])

Table 2 Notations used in Sect. 2.2

V_{in}, I_{in}	Input voltage and current of converter
V_{out}, I_{out}	Output voltage and current of converter
η_{conv}	Efficiency of the converter
P_{conv}	Power loss of the converter
D	PWM duty ratio
ΔI	Maximum current ripple of converter
f_s	The switching frequency
$I_{\text{controller}}$	Current of the microcontroller
R_L, R_C	Internal series resistances of inductor and capacitor
$R_{\text{sw},i}$, $Q_{\text{sw},i}$	Resistance and gate charge of the ith MOSFET

V_{out}, the charger operates in one of the two possible operating modes: the buck mode when $V_{\text{in}} > V_{\text{out}}$ and the boost mode otherwise [2, 3].

Power conversion is not free. Converting the voltage level involves nonzero amount of power loss. The overall power loss includes conduction losses by parasitic resistances of circuit components, switching losses by parasitic capacitances of switching devices, power consumption of the controller circuit, and so on. The power conversion efficiency η_{conv} is defined as:

$$\eta_{\text{conv}} = \frac{V_{\text{out}} \cdot I_{\text{out}}}{V_{\text{in}} \cdot I_{\text{in}}} = \frac{V_{\text{in}} \cdot I_{\text{in}} - P_{\text{conv}}}{V_{\text{in}} \cdot I_{\text{in}}} \tag{4}$$

where P_{conv} denotes the power loss in the converter/charger. This power loss is not constant, but varies depending on the input and output voltages and the amount of power that is transferred through the converter, and thus, the power conversion efficiency is also a variable. The power conversion efficiency is a critical factor because it determines the amount of harvested PV energy that can be ultimately transferred to the storage system (and to be used later.) In general, the power conversion efficiency will be maximized when (i) the input voltage and output voltage are close to each other, and (ii) the output current is within a certain desirable range.

We develop the converter power model based on the power model for buck switching converter provided in [2]. When the charger/converter is operating in the buck mode, its power loss P_{conv} is given by:

$$P_{\text{conv}} = (I_{\text{out}})^2 \cdot (R_L + D \cdot R_{\text{sw},1} + (1 - D) \cdot R_{\text{sw},2} + R_{\text{sw},4}) \tag{5}$$

$$+ \frac{(\Delta I)^2}{12} \cdot (R_L + D \cdot R_{\text{sw},1} + (1 - D) \cdot R_{sw,2} + R_{sw,4} + R_C) \tag{6}$$

$$+ V_{\text{in}} \cdot f_s \cdot (Q_{\text{sw},1} + Q_{\text{sw},2}) + V_{\text{in}} \cdot I_{\text{controller}} \tag{7}$$

where $D = V_{\text{out}}/V_{\text{in}}$ is the PWM duty ratio and $\Delta I = V_{\text{out}} \cdot (1 - D)/(L \cdot f_s)$ is the maximum current ripple; f_s is the switching frequency; $I_{\text{controller}}$ is the current of the microcontroller of the charger; R_L; and R_C are the internal series resistances of the inductor L and the capacitor C, respectively; $R_{\text{sw},i}$ and $Q_{\text{sw},i}$ are the turn-on resistance and gate charge of the ith MOSFET switch shown in Fig. 4, respectively.

The charger power loss P_{conv} in the boost mode is given by:

$$P_{\text{conv}} = \left(\frac{I_{\text{out}}}{1-D}\right)^2 \cdot (R_L + D \cdot R_{\text{sw},3} + (1-D) \cdot R_{\text{sw},4} + R_{\text{sw},1} + D(1-D)R_C) \tag{8}$$

$$+ \frac{(\Delta I)^2}{12}(R_L + D \cdot R_{\text{sw},3} + (1-D)(R_{\text{sw},4} + R_C) + R_{\text{sw},1}) \tag{9}$$

$$+ V_{\text{out}} \cdot f_s \cdot (Q_{\text{sw},3} + Q_{\text{sw},4}) + V_{\text{in}} \cdot I_{\text{controller}} \tag{10}$$

where $D = 1 - V_{\text{in}}/V_{\text{out}}$ and $\Delta I = V_{\text{in}} \cdot D/(L \cdot f_s)$.

The power dissipation of the charger is minimized when (i) the input voltage and the output voltage of the charger are close to each other and (ii) the output current of the charger is within a certain range. Let $I_{\text{out}} = \text{Chg\_Out\_}I(V_{\text{in}}, I_{\text{in}}, V_{\text{out}})$ denote the function that calculates I_{out} based on V_{in}, I_{in}, and V_{out}.

2.3 Mitigating the Output Variation of PV Modules

2.3.1 Maximum Power Point Tracking

As discussed in Sect. 2.1, the output current of a PV cell is a function of the output voltage of the PV cell; hence, the resultant output power also varies by the voltage. As a result, the voltage-dependent output power is maximized only at a certain operating point, which is called the MPP. Since the V-I curve of a PV cell varies by irradiation level on the cell and the temperature of the cell, the MPP of the PV cell also changes by these factors. In order to generate the maximum power from PV cells, the operating point should be dynamically adjusted to remain at their MPP adaptive to the changes in the irradiance level and temperature. This technique for finding the MPP and adjusting the operating point to it is called the MPPT, and it is mandatory for realizing energy-efficient PV systems.

There are numerous research efforts on MPPT techniques [4]. A brute force technique is sweeping all the voltage levels from short-circuit to open-circuit to find the optimal voltage level. However, it takes a long time to find the optimal voltage, and it suffers from low power generation during the sweeping operation. Another simple yet effective technique is utilizing the precharacterized V-I curve

of the PV cell to predict the irradiance level and find the optimal voltage. Other MPPT techniques perform feedback control of the system to adjust the operating point. For example, perturb and observe (P&O) technique, or hill-climbing technique, makes a slight increase or decrease (perturbation) in the PV cell voltage to see which direction increases the output power (observe), and change the operating voltage in that way. Incremental conductance techniques utilize the property that $\mathrm{d}P^{\mathrm{pvc}}/\mathrm{d}V^{\mathrm{pvc}} = 0$ at the MPP. It compares the incremental conductance ($\mathrm{d}I^{\mathrm{pvc}}/\mathrm{d}V^{\mathrm{pvc}}$) and the PV cell's instantaneous conductance ($I^{\mathrm{pvc}}/V^{\mathrm{pvc}}$) to determine whether to increase or decrease V^{pvc}. Surveys on various MPPT techniques can be found from [5, 6].

2.3.2 Maximum Power Transfer Tracking

While the MPPT techniques are essential to maximize the power obtained from PV cells, it may not be the true optimal solution from the perspective of the whole system. The energy eventually consumed by a load or stored in an energy storage device is the output of the power converter, not the output power of the PV cells. As presented in Sect. 2.2, the power conversion efficiency of a power converter is not 100 %, but it is variable depending on the input and output conditions. Since the output of PV cells becomes the input of the power converter, the operating point of the PV cells affects the efficiency of the power conversion. By the use of an MPPT technique, we can maximize only the input power to the converter, which, however, does not guarantee the maximum output power from the converter. In addition, the output of the converter, which is a load device or an energy storage, is also subject to significant variation. For example, the terminal voltage of a supercapacitor changes linearly proportional to its state of charge. Therefore, the system-level energy-optimal design and operation of a PV system must take account of the variable efficiency.

Figure 5 is a conceptual graph that shows how the conversion efficiency affects the power harvested from a PV cell. The output power from the PV cell, which is the input power to the converter is maximum when the PV output voltage is at (A), and this point is the MPP. However, due to the variation of the conversion efficiency as denoted by the dotted curve, the converter output power, which is

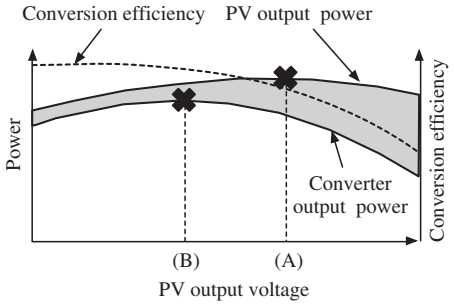

Fig. 5 PV output power and converter output power variation by PV output voltage. Shaded area denotes the power loss in the converter

the amount that we can actually utilize at the load, has a different maximum point, (B). This point is called the maximum power transfer point, or the MPT point, and we can maximize the net power by operating the PV cell at this point. The techniques for dynamically adjusting the operating point to the MPT point is called the maximum power transfer tracking (MPTT) [7]. The MPTT requires considerations not only on the characteristics of the PV cell, but also on the characteristics of the power converter, the load, and the storage device, all together.

In this context, some recent research efforts have recognized the impact of the power conversion efficiency and proposed novel circuits for maximizing the output power [8–11]. These output-maximizing converters are proposed to address the suboptimality of the conventional MPPT power converters. They have a feedback control loop that monitors the output of the power converter. Unlike the MPPT power converters that monitor the PV cell output, these converters monitor the converter output and adjust the operating point, e.g., the operating frequency of a charge pump.

More recently, MPTT-aware system design optimization techniques have been proposed. These techniques recognize the impact of components optimization in design time to the energy efficiency, such as the configuration of PV cell array or supercapacitor array. In [7], it is shown that the amount of energy harvesting may vary greatly depending on the PV array configuration and the capacitance of the supercapacitor. They proposed an optimization framework that finds the most cost-efficient PV array configuration and the most energy-efficient capacitance for a given requirement on the amount of energy. A technique proposed in [12] involves both a design-time optimization and a runtime reconfiguration technique. In design time, several supercapacitors of different capacitances are evaluated to find the best capacitance that maximizes energy efficiency. During operation, the array of the supercapacitors is dynamically reconfigured to change the terminal voltage and effective capacitance adaptively. In [13], a cross-layer optimization method is introduced, which derives the optimal design parameters such as PV cell silicon thickness, PV cell array configuration, and charge pump stages and frequency.

2.4 Partial Shading and PV Cell Faults

In reality, the solar irradiance levels received by PV cells in a PV system may be different from each other when a portion of PV modules is in shadow, and such a phenomenon is known as the partial shading effect. For example, moving clouds cause partial shading for stationary applications. On the other hand, shadows from nearby objects (e.g., buildings, trees, and poles) produce partial shading for PV systems on hybrid electric vehicles, which is much more severe as vehicles are moving through shaded or lighted regions. In these cases, the partial shading pattern may be quite regular (i.e., like a block), and we call this case *block shading*. Partial shading may also result from fallen leaves or dust on the PV modules [14], or other aging effects of PV modules. In this case, the partial shading pattern may

be randomized, and we call this case *random shading*. Moreover, PV cell faults, which make the output of the faulty PV cell to zero, have similar impact as the partial shading effect.

PV cells generally have different MPPs under the partial shading effect. Partial shading not only reduces the maximum output power of the shaded PV cells, but also makes the lighted or less-shaded PV cells that are connected in series with the shaded ones to deviate from their MPPs. In other words, the PV cells cannot simultaneously operate at their MPPs. With partial shading, the maximum output power of a PV module becomes much lower than the sum of the maximum output power values of all the individual PV cells in the PV module.

We demonstrate that the partial shading effect or PV cell faults may significantly degrade the output power level of a PV module with a fixed $n \times m$ configuration. We use a PV module with a 2×2 configuration as an example. As shown in Fig. 6, the PV module consists of two series-connected PV groups, and each PV group consists of two parallel-connected PV cells. The PV cell at the bottom right is completely shaded (with no solar irradiance, or has a PV cell fault) while the rest of PV cells receive the solar irradiance under the standard test condition i.e., G_{STC} W/m^2. Since only one PV cell out of four is shaded, the ideal setup should exhibit the PV module output power degradation of 25 % compared to the same PV module without any shading. However, the actual PV module output power degradation is much larger than 25 %.

We plot in Fig. 7 the V-I characteristics of the PV module under partial shading (or PV cell fault). Curve 1 corresponds to the V-I output characteristics of the bottom PV group with the shaded PV cell, whereas Curve 2 corresponds to the V-I output characteristics of the top PV group. Curve 2 has a higher current value than Curve 1 at the same voltage value. Curve 3 is the V-I output characteristics of the PV module, which is directly derived from Curves 1 and 2 since the PV module is a series connection of the two PV groups. Note that we assume that each PV cell is integrated with a bypass diode to protect the PV cell from reverse bias operation under partial shading [15] when we derive Curve 3.

We compare the end-to-end V-P output characteristics of the partially shaded PV module (or PV module with PV cell fault) with the same PV module without

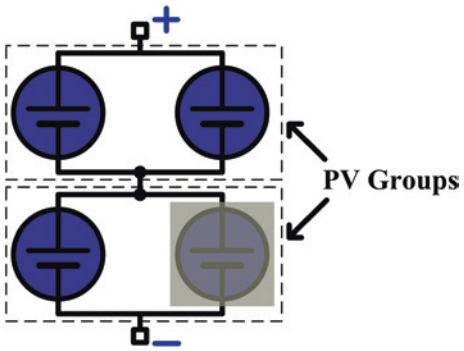

Fig. 6 An example of partial shading on a PV module with four PV cells (Reproduced with permission from Wang et al. [22])

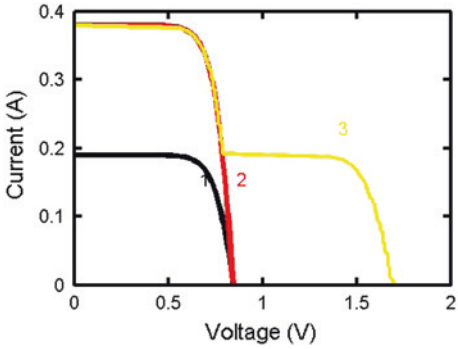

Fig. 7 V-I characteristics of the PV module under partial shading

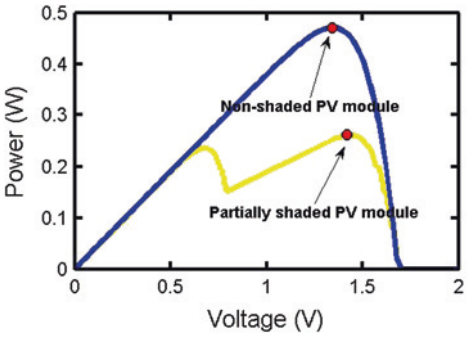

Fig. 8 V-P characteristics of the PV module under partial shading

shading in Fig. 8. The red dots in Fig. 8 show the MPPs. The maximum output power of the partially shaded PV module (or PV module with PV cell fault) is about 56 % of that of the same PV module without shading (or PV cell fault). As a result, one shaded (or faulty) PV cell degrades the PV module output power by as much as 44 %, which establishes the significance of the effect of partial shading effect (or PV cell fault).

In addition, partial shading (or PV cell fault) may result in multiple power peaks in the V-P output characteristics of a PV module, as also can be seen in Fig. 8. Therefore, the MPPT (or MPTT) techniques must be modified in order to dynamically track a global optimum operating point instead of a local optimal one [16, 17]. This is because the existing MPPT or MPTT techniques such as the perturb and observe method rely on the unimodality assumption about the V-P output characteristics of the PV module. The modified MPPT or MPTT techniques increase the complexity of the PV system control circuitry.

The modified MPPT techniques may restore part of the power loss due to partial shading, but they cannot fully utilize the lighted PV cells due to the deviation from their MPPs caused by the shaded cells. On the other hand, PV module reconfiguration techniques, which have the potential of fully exploiting the MPPs of both lighted and shaded PV cells in a partially shaded PV module, can help maintain the output power level of a PV system under partial shading. Various

PV reconfiguration techniques have been proposed, which are different from each other in terms of the system structure and control approach that they employ [18–20]. However, they suffer from one or more of the following limitations:

1. To compensate the power loss from shaded PV cells, many extra PV cells are needed for performing reconfiguration according to the shading pattern.
2. There is a lack of systematic and scalable structural support or effective control mechanism.
3. Variations in the conversion efficiency of the charger or inverter at different operating points are overlooked, which may result in a sizeable degradation in the overall energy conversion efficiency.

3 Reconfigurable Photovoltaic Cell Array

In this section, we introduce a reconfigurable PV cell array architecture and its operation. Reconfigurable PV cell arrays have several benefits when compared with fixed (nonreconfigurable) PV cell arrays. First, the output voltage and current of PV cell arrays can be adjusted so that the efficiency of the power converter is maximized. Second, the effects of partial shading can be mitigated. Third, faulty cells can be dynamically excluded from PV cell arrays without service interruption. We first introduce the switch network architecture of the reconfigurable PV cell array, and then, we describe its benefits in the rest of this section.

3.1 Reconfigurable Switch Network Architecture

In most cases, the output of a single PV cell can generate no more than a few watts. Therefore, it is typical to connect multiple PV cells to build a PV cell array to obtain a higher output voltage and/or a higher output current. Stacking PV cells in series increases the output voltage, while multiple PV cells in parallel increases the output current. It is important to properly design the number of series and parallel connections to obtain desired voltage and current levels. However, the optimal configuration that produces the maximum power changes by irradiance level, temperature, storage device state of charge, and so forth, as we discussed in Sect. 2.3.2. Therefore, instead of fixing the configuration, it is beneficial to be able to dynamically change the configuration during operation as needed. In [21], a switch network architecture for dynamic array reconfiguration is introduced. It is originally proposed for the reconfiguration of an energy storage array, e.g., supercapacitor array or battery array, but it can be leveraged for the reconfiguration of PV cell arrays in the same manner.

Figure 9 shows the reconfigurable switch network architecture for a PV cell array that consists of N PV cells, $C_{1,\ldots,N}$. First $N-1$ cells, from C_1 to C_{N-1}, have

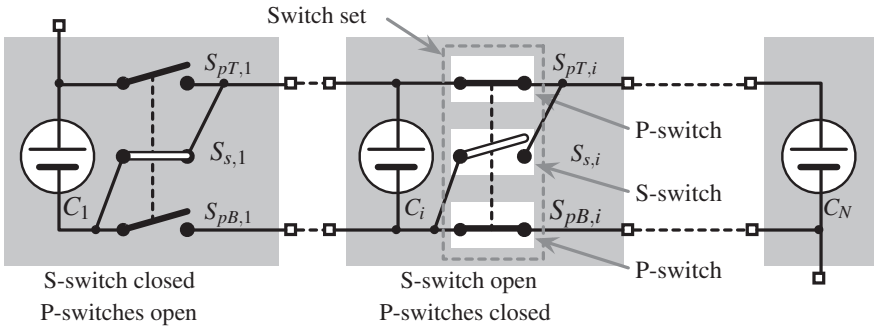

Fig. 9 Reconfigurable switch network architecture [21]

a set of three switches each. One switch set is composed of one series switch (S-switch) and two parallel switches (P-switches). The S-switch of the ith cell is denoted by $S_{s,i}$, and the two P-switches of the ith cell are denoted by $S_{pT,i}$ (top parallel switch) and $S_{pB,i}$ (bottom parallel switch).

There are a few rules for the operation of the three switches in a switch set:

- Two paired P-switches should be open or closed at the same time.
- Either S-switch or P-switches pair should be closed at any moment.
- S-switch and P-switches pair should not be closed at the same time.

More formally, for $i = 1, 2, \ldots, N-1$,

$$x_{p,i} + x_{s,i} = 1, \tag{11}$$

where the binary variables $x_{p,i}$ and $x_{s,i}$ are defined as

$$x_{s,i} = \begin{cases} 0 \text{ if } S_{s,i} \text{ is open,} \\ 1 \text{ if } S_{s,i} \text{ is closed,} \end{cases} \tag{12}$$

$$x_{P,i} = \begin{cases} 0 \text{ if } S_{pT,i} \text{ and } S_{pB,i} \text{ are open,} \\ 1 \text{ if } S_{pT,i} \text{ and } S_{pB,i} \text{ are closed.} \end{cases} \tag{13}$$

One and only one of $x_{s,i}$ and $x_{p,i}$ should be 1 at any moment. If both $x_{s,i}$ and $x_{p,i}$ are 1 at the same time, C_i is short circuited. On the other hand, if both $x_{s,i}$ and $x_{p,i}$ are 0 at the same time, C_i is disconnected from C_{i+1}.

Consecutive PV cells that are connected in series form a PV group. All the PV cells in the same PV group are connected in series; hence, the current through these PV cells is all identical. Multiple PV groups are connected to their adjacent PV groups in parallel. Therefore, the terminal voltage of all the PV groups becomes identical.

3.2 Balanced Configurations

A PV cell array configuration that all the PV groups have the same number of PV cells is called a *balanced configuration*. If the solar irradiance onto every PV cell is uniform, the output voltage and current of each PV cell are also uniform in a balanced configuration. As balanced configurations are the most basic configurations of a PV array, we first discuss their properties in this subsection. Then we discuss imbalanced configurations, where the number of PV cells in each PV group may differ, in the following subsection.

The flexibility of the reconfigurable switch architecture introduced in Sect. 3.1 allows any arbitrary balanced configuration. The number of feasible balanced configurations that we can make using N PV cells is equivalent to the number of divisors of N. For example, the number of balanced configurations of a 10-cell PV cell array ($N = 10$) is four: 10×1, 5×2, 2×5, and 1×10, where $m \times n$ is the m -series and n-parallel balanced configuration. Note that the number of divisors of 10 is four: 1, 2, 5, and 10.

Using the binary variables $x_{s,i}$ and $x_{p,i}$ defined in Sect. 3.1, the balanced configurations of a $m \times n$ PV cell array are obtained by switching operations which obey the following rule:

$$x_{s,i} = \begin{cases} 1 \text{ if } i = n \cdot k \text{ where } k = 1, 2, \ldots, m-1, \\ 0 \text{ otherwise,} \end{cases} \tag{14}$$

$$x_{p,i} = 1 - x_{s,i}. \tag{15}$$

Assuming that the solar irradiance is uniform across the whole PV cell array, the output voltage V_{pvm} and the output current I_{pvm} of a balanced $m \times n$ PV cell array are:

$$V_{\text{pvm}} = m \times V_{\text{pvc}}, \tag{16}$$

$$I_{\text{pvm}} = n \times I_{\text{pvc}}. \tag{17}$$

Figure 10 is the balanced configurations that we can make using a 4-cell PV cell array ($N = 4$). It shows three balanced configurations: 4×1, 2×2, and 1×4. For example, the 2×2 configuration consists of two PV groups, each of which is composed of two PV cells connected in parallel with a pair of P-switches, and the two groups are connected in series with a S-switch.

Recall that the amount of energy harvested from a PV cell array may vary depending on its configuration even if the number of PV cells is the same. Finding the optimal configuration was a part of the optimization framework introduced in [7], but this was a static design-time decision. However, the optimal configuration that maximizes the power delivered to the load or storage device keeps changing as we discussed in 2.3.2. We can leverage this PV cell array reconfiguration architecture to further improve the energy delivery by dynamically reconfiguring the PV array in runtime.

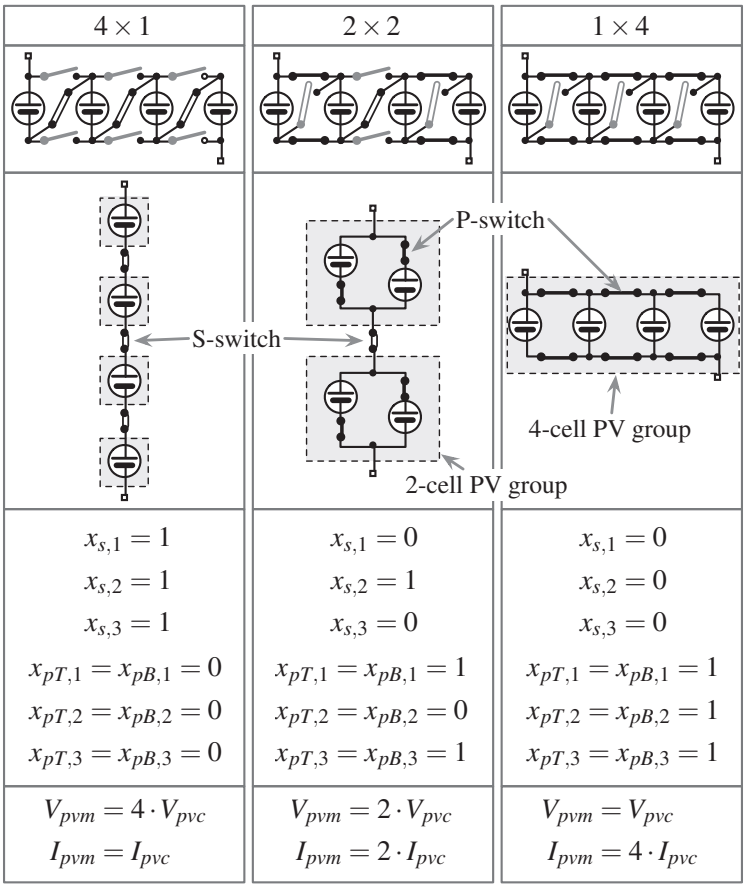

Fig. 10 Balanced configurations of a four-cell PV cell array ($N = 4$)

3.3 Imbalanced Reconfiguration to Combat Partial Shading

In general, a reconfigurable PV array (module) with N PV cells can achieve imbalanced reconfiguration, i.e., it can have a arbitrary number (less than or equal to N) of PV groups, each with arbitrary number of PV cells with consecutive IDs. Figure 11 is an example of PV module reconfiguration. The first four PV cells are connected in parallel to form PV Group 1; the next three PV cells form PV Group 2; and the last five PV cells form PV Group 3. These three PV groups are series-connected by the S-switches of the fourth and the seventh PV cells.

A reconfigurable PV module consisting of N PV cells may include an arbitrary number (less than or equal to N) of PV groups. The number of parallel-connected PV cells $r_j (> 0)$ in the jth PV group should satisfy

$$\sum_{j=1}^{g} r_j = N, \tag{18}$$

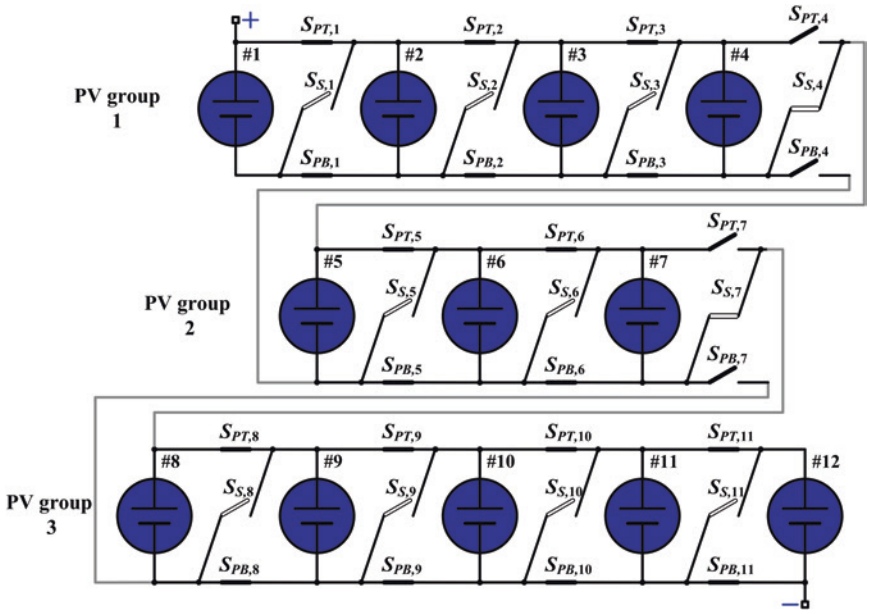

Fig. 11 An imbalanced reconfiguration example (Reproduced with permission from Wang et al. [22])

where g is the number of PV groups. This configuration can be viewed as a partitioning of the PV cell index set $\mathbf{A} = \{1, 2, 3, \ldots N\}$, where the elements in $\mathbf{A}$ denote the indices of PV cells in the array. This partitioning is denoted by subsets $\mathbf{B}_1$, $\mathbf{B}_2$,…, and $\mathbf{B}_g$ of $\mathbf{A}$, which correspond to the g PV groups comprised of r_1, r_2, …, and r_g PV cells, respectively. The subsets $\mathbf{B}_1$, $\mathbf{B}_2$, …, and $\mathbf{B}_g$ satisfy

$$\cup_{j=1}^{g} \mathbf{B}_j = \mathbf{A} \tag{19}$$

and

$$\mathbf{B}_j \cap \mathbf{B}_k = \emptyset, \quad \forall\, j,k \in \{1, 2, \ldots, g\}, \;\; j \neq k \tag{20}$$

The indices of PV cells in group j must be smaller than the indices of PV cells in group k for any $1 \leq j < k \leq g$ due to the structural characteristics of the reconfigurable PV array, i.e., $i_1 < i_2$ for $\forall\, i_1 \in \mathbf{B}_j$ and $\forall\, i_2 \in \mathbf{B}_k$ satisfying $1 \leq j < k \leq g$. A partitioning satisfying the above properties is called an *alphabetical partitioning*.

Figure 12 shows the architecture of a PV system with a reconfigurable PV array (module), equipped with the reconfiguration architecture. The input and output ports of the charger are connected to the PV module and a supercapacitor array, respectively. The charger regulates the operation of the PV module by regulating its output voltage. The output current of the PV module is automatically determined based on its V-I characteristics. We adopt a software-based MPTT

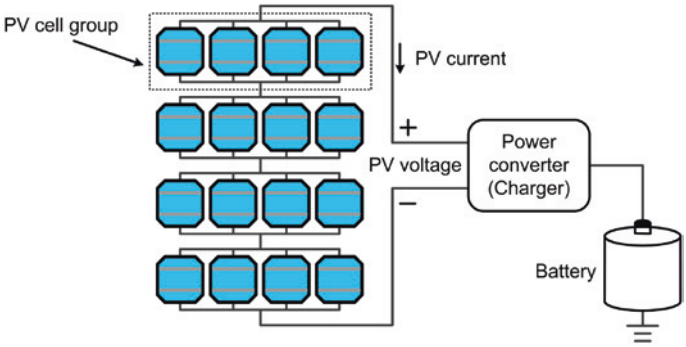

Fig. 12 The system structure of the reconfigurable PV system (Reproduced with permission from Lin et al. [23])

technique in the proposed PV system. It employs the perturb & observe (P&O) algorithm to maximize the charger output current through regulating the output voltage of PV module.

For the ith PV cell, the relationship between output voltage V_i^{pvc} and output current I_i^{pvc} depends on the solar irradiance G_i as given by PV cell characteristics. We obtain G_i of each PV cell using onboard solar irradiance sensors. The PV cell temperature has a relatively minor effect on the V-I characteristics.

The output voltage and current of the PV module are denoted by V_{pv} and I_{pv}, respectively. The power consumption of the charger is P_{conv}. The terminal voltage of the supercapacitor is V_{cap}, and the charging current of the supercapacitor is I_{cap}. We have

$$V_{\text{pv}} \cdot I_{\text{pv}} = P_{\text{conv}} + V_{\text{cap}} \cdot I_{\text{cap}}. \tag{21}$$

We provide a formal problem statement for the PV module reconfiguration (PMR) problem in the following.

PMR Problem Statement: Given G_i of each ith PV cell and V_{cap}, **find** the optimal configuration of the PV module and the optimal operating point $(V_{\text{pv}}, I_{\text{pv}})$, **such that** I_{cap} is maximized. The objective is equivalent to maximizing the PV system output power.

We propose the near-optimal PV module reconfiguration algorithm comprised of a kernel algorithm and an outer loop. The kernel algorithm finds the optimal number of PV cells in each PV group with a given group number g such that the PV module MPP power is maximized. The kernel algorithm is based on dynamic programming with polynomial time complexity. The outer loop determines the optimal g value.

With details shown in [22], the kernel algorithm relies on the observation that the MPP voltages of a PV cell under different solar irradiance levels are very close to each other, but the corresponding MPP currents vary significantly. Let $V_{\text{pvc}}^{\text{MPP}}$ denote the solar irradiance-independent MPP voltage of a PV cell, and let $I_{\text{pvc}}^{\text{MPP}}(G)$

denote the MPP current as a function of the solar irradiance G. The kernel algorithm maximizes the estimated PV module MPP power as given by

$$g \cdot V_{\text{pvc}}^{\text{MPP}} \cdot \min_j \sum_{i \in \mathbf{B}_j} I_{\text{pvc}}^{\text{MPP}}(G_i) \tag{22}$$

Or equivalently, it maximizes $\min_j \sum_{i \in \mathbf{B}_j} I_{\text{pvc}}^{\text{MPP}}(G_i)$. Optimal substructure property with details shown in [22] applies to this problem. Hence, we apply dynamic programming method as the basis of the kernel algorithm to solve this problem. Details of the kernel algorithm are provided in [22].

In the outer loop, we first execute the kernel algorithm to find an optimal configuration for a given group number g value. After that, we calculate the estimated I_{cap} under such configuration using the charger characteristics. In the calculation of the estimated I_{cap}, we estimate the PV module output voltage and current by $g \cdot V_{\text{pvc}}^{\text{MPP}}$ and $\min_j \sum_{i \in \mathbf{B}_j} I_{\text{pvc}}^{\text{MPP}}(G_i)$, respectively. We find the optimal g value that maximizes the estimated I_{cap}, and the corresponding configuration subsequently. Details are provided in [22].

3.4 Fault Tolerance

3.4.1 Reconfiguration for Fault Detection and Fault Bypassing

The objective of fault detection is to identify any PV cell faults in the PV panel. Fault bypassing aims at forming a new PV panel configuration to minimize the output power loss caused by PV cell faults [23]. Consider a PV panel assuming a $N \times M$ configuration during normal system operation. For fault detection, we may need to form a $k \times M$ PV panel configuration ($k \leq N$) with a selected set of PV cells and measure their combined output power to determine whether a PV cell fault exists in this portion of PV panel. During fault bypassing, we may need to form a $N_{\text{opt}} \times M_{\text{opt}}$ PV panel configuration to improve the system output power, where the faulty PV cells, and perhaps some healthy PV cells are excluded from the new configuration $N_{\text{opt}} \times M_{\text{opt}} < N \times M$.

Inactivating even healthy PV cells may become necessary in some cases of fault bypassing. For example, suppose we have 42 PV cells and one of them is faulty. We cannot form a good configuration with a prime number of 41 healthy PV cells such that the MPP voltage of this configuration matches with the battery voltage. Therefore, we would like to inactivate one healthy PV cell to have 40 active cells. Then we are able to perform a 5×8 or 8×5 configuration to increase the PV system output power. The inactivated healthy PV cell may be used later if we encounter an additional PV cell fault.

We use Fig. 13 as an example to illustrate how to effectively control the ON/OFF states of the switches for fault detection and fault bypassing. PV cells 1, 5, and 16 are inactive healthy PV cells, and PV cell 8 is a faulty PV cell. Figure 13

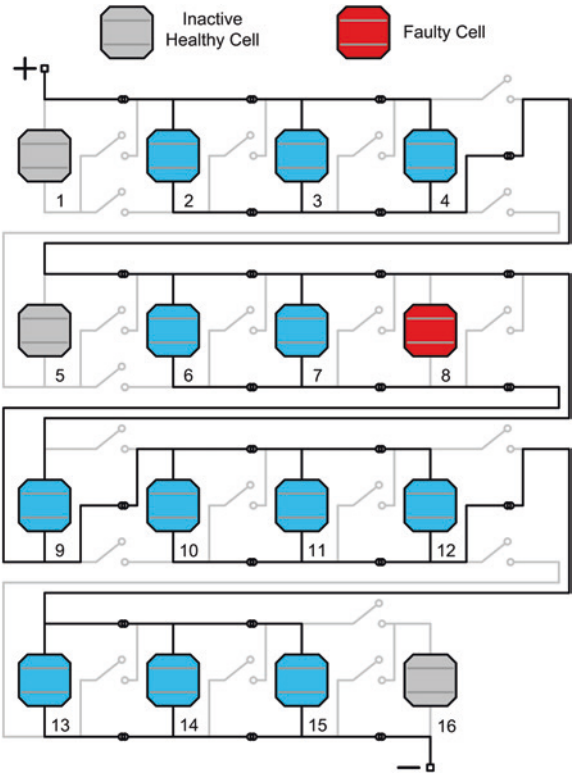

Fig. 13 An example of PV reconfiguration for fault detection and fault bypassing (Reproduced with permission from Lin et al. [23])

shows a 4 × 3 PV panel configuration formed with the remaining PV cells. The faulty PV cell 8 is open-circuited and inactive outside our control. The healthy PV cells can be isolated in either of two cases: (i) they are located between two PV cell groups; (ii) they are at the leftmost or the rightmost position in the electrical connection of the PV panel. In Fig. 13, an example of the first case is PV cell 5, whereas examples of the second case are PV cells 1 and 16.

The fault detection and bypassing algorithms for fault-tolerant PV systems are proposed based on the reconfigurable PV panel structure. The fault detection algorithm can identify a PV cell fault with logarithmic time complexity or determine the nonexistence of a PV cell fault in O(1) time. The fault bypassing algorithm determines the optimal configuration of a PV panel, such that the PV system output power degradation due to PV cell faults can be minimized.

The fault detection algorithm is executed every Δt units of time. Δt must be much smaller than the average fault occurrence time interval, which is in the order of days or months, so that we can safely assume that at most one PV cell fault occurs during each time interval and the fault detection algorithm only needs to detect at most one newly occurring fault at each execution. The fault detection algorithm first compares the actual PV panel output power with the theoretical output power of the PV panel without any faults. If the difference is smaller

than a prespecified error threshold, then there will exist no new fault, and the fault detection algorithm will terminate in O(1) time. Otherwise, the fault detection algorithm will continue to find the fault, and the fault bypassing algorithm will be executed. In most cases, the fault detection algorithm will confirm the nonexistence of a new fault. Therefore, the computational overhead of the fault detection and bypassing algorithms is small. In practice, we have found that Δt can be set to an hour.

3.4.2 Fault Detection Algorithm

The basic step of the fault detection algorithm is the *Fault Existence Checking* algorithm, which determines whether a PV cell fault exists in a set of $k \times M$ PV cells. We track the maximum output power of the $k \times M$ PV panel configuration using the charger in the PV system at Step 3 of the Fault Existence Checking algorithm. In reality, k must be larger than or equal to a threshold value $K_{\min}$ such that the output voltage of the $k \times M$ PV panel configuration is high enough to properly drive the charger. This means that the Fault Existence Checking algorithm cannot run on a PV panel configuration smaller than $K_{\min} \times M$.

The fault detection algorithm has two steps: first, determine which row the faulty PV cell is located at (row search); second, determine which column the faulty PV cell is located at (column search). To find the location of the potential faulty PV cell in the $N \times M$ PV panel, we first run the Fault Existence Checking algorithm on the whole PV panel. If it is confirmed that no PV cell fault exists, the fault detection algorithm will terminate. Otherwise, the fault detection algorithm will continue to find the location of the PV cell fault as explained next. Detailed procedure is described in Algorithm 1.

We use Fig. 14 to demonstrate how the row search and column search proceed. In this example, $N = 4$, $M = 4$, and $K_{\min} = 2$. For row search, we bisect the PV panel into the first two rows (A1) and the remaining two rows (A2). We run the Fault Existence Checking algorithm on A1 and find out that A1 contains a faulty PV cell. Then we bisect A1 into the first row (B1) and the second row (B2). The size of B1 is smaller than $K_{\min} \times M$. Therefore, we form a $K_{\min} \times M$ (2×4) configuration from B1 along with the third row, which has been confirmed to contain only healthy PV cells, and subsequently, run the Fault Existence Checking algorithm on this configuration. We determine that B1 does not contain the faulty PV cell, and therefore, the faulty PV cell is within B2. Now, we have located the row containing the faulty PV cell.

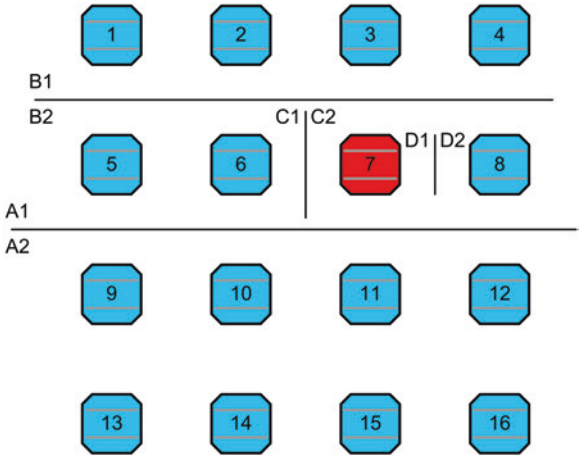

Fig. 14 Illustration of the fault detection algorithm (Reproduced with permission from Lin et al. [23])

Algorithm 1: Finding the Location of the PV Cell Fault

$\mathbf{V_{com}} \leftarrow$ the $N \times M$ PV module; $k \leftarrow N$
while $k > 1$ **do**
  $\mathbf{V_{part1}} \leftarrow$ the first $k_1 = \lfloor k/2 \rfloor$ rows in $\mathbf{V_{com}}$
  $\mathbf{V_{part2}} \leftarrow$ the rest $k_2 = k - \lfloor k/2 \rfloor$ rows in $\mathbf{V_{com}}$
  if $k_1 \geq K_{min}$ **then**
    $R \leftarrow$ Run Fault Existence Checking on $\mathbf{V_{part1}}$
    If $R = 1$: $\mathbf{V_{com}} \leftarrow \mathbf{V_{part1}}$; $k \leftarrow k_1$
    Else: $\mathbf{V_{com}} \leftarrow \mathbf{V_{part2}}$; $k \leftarrow k_2$
  else
    $\mathbf{V_b} \leftarrow K_{min} - k_1$ rows of PV cells that have been confirmed to be healthy PV cells
    $R \leftarrow$ Run Fault Existence Checking on $\mathbf{V_{part1}}$ along with $\mathbf{V_b}$
    If $R = 1$: $\mathbf{V_{com}} \leftarrow \mathbf{V_{part1}}$; $k \leftarrow k_1$
    Else: $\mathbf{V_{com}} \leftarrow \mathbf{V_{part2}}$; $k \leftarrow k_2$
$\mathbf{V_{com}}$ is now the row containing the faulty PV cell
while $k > 1$ **do**
  $\mathbf{V_{part1}} \leftarrow$ the first $k_1 = \lfloor k/2 \rfloor$ cells in $\mathbf{V_{com}}$
  $\mathbf{V_{part2}} \leftarrow$ the rest $k_2 = k - \lfloor k/2 \rfloor$ cells in $\mathbf{V_{com}}$
  $\mathbf{V_b} \leftarrow K_{min} \times M - k_1$ PV cells that have been confirmed to be healthy PV cells
  $R \leftarrow$ Run Fault Existence Checking on $\mathbf{V_{part1}}$ along with $\mathbf{V_b}$
  If $R = 1$: $\mathbf{V_{com}} \leftarrow \mathbf{V_{part1}}$; $k \leftarrow k_1$
  Else: $\mathbf{V_{com}} \leftarrow \mathbf{V_{part2}}$; $k \leftarrow k_2$
Return $\mathbf{V_{com}}$

For column search, we bisect B2 into PV cells 5 and 6 (C1) and PV cells 7 and 8 (C2). We run the Fault Existence Checking algorithm on C1 along with PV cells 3, 4, and 9–12 that are confirmed healthy. We pick these healthy PV cells, because in this way we can form a 2 × 4 configuration, with PV cells 7 and 8 bypassed between the first PV cell group (PV cells 3–6) and the second PV cell group (PV

cells 9–12). We find out that C1 does not contain the faulty PV cell, and therefore, C2 contains the faulty PV cell. We bisect C2 into PV cell 7 (D1) and PV cell 8 (D2). We form a 2×4 configuration from D1 along with PV cells 4–6 and 9–12, and run the Fault Existence Checking algorithm on this configuration. We confirm that the faulty PV cell is PV cell 7, and thereby, conclude the column search.

3.4.3 Fault Bypassing Algorithm

The fault bypassing algorithm determines the optimal configuration of a PV panel, such that the PV system output power loss due to PV cell faults is minimized. We need to decide (i) the number of active healthy PV cells S, and (ii) the optimal PV panel configuration $N_{\text{opt}} \times M_{\text{opt}}$. Let us denote the number of factors of S by $F(S)$. The maximum output power of a PV panel is approximately proportional to S. And a S value is preferred if $F(S)$ is larger, since we have more choices of PV panel configurations with this S value.

Algorithm 2: Fault Bypassing Algorithm of a PV Panel

Input: G, T, and V_{bat}
Output: N_{opt} and M_{opt}
1 $I_{bat}^{max} \leftarrow 0$
2 Determine the set of candidate S values
3 **for** *each S value in the candidate set* **do**
4 **for** N' *from 1 to S* **do**
5 **if** $M' = S/N'$ *is an integer* **then**
6 Calculate I_{bat} from M', N', V_{bat} and Chg_Out_I function
7 Update I_{bat}^{max}, N_{opt}, M_{opt} if $I_{bat} > I_{bat}^{max}$

Assume that the PV panel has $N \times M$ PV cells and L PV cell faults have been identified so far. Therefore, we have $S_{\max} = N \times M - L$. First, we determine a set of candidate S values in ascending order, which satisfies $S + F(S) \geq S_{\max} + F(S_{\max})$. There are $F(S)$ possible configurations using S active healthy PV cells. Among these configurations, there exists an optimal configuration that provides maximum PV system output power $P_{\max}(S)$. Based on the PV cell and charger model, we find the optimal S_{opt} value by ternary search on the set of candidate S values, such that $P_{\max}(S_{\text{opt}})$ is the maximum achievable PV system output power. The optimal PV panel configuration is determined accordingly. Detailed procedure is described in Algorithm 2.

4 Storage- and Converter-Less Energy Harvesting

Energy storage elements as well as power converters have been necessary components for performing an MPPT. However, as described, these components seriously limit the design and implementation of load devices in many aspects including the weight, form factor, cost, maintainability, etc. In addition, using those components may result in additional energy loss while storing the energy and converting the voltage level as described in the previous sections. So elimination of those components gives numerous benefits for designing load devices. This section mainly focuses on introducing a breakthrough MPPT method without neither power converters nor energy storage elements for low-power PV energy harvesting applications.

4.1 Principle of Operation

There are obvious obstacles in eliminating power converters and energy storage elements from the conventional energy harvesting devices. First, the MPP current and voltage should be exactly matched with the operating ranges of the load devices without using those two components. However typical electronic components including microprocessors, in general, are unable to fulfill this requirement by themselves. Second, the load devices should be functional even after power interruption when the PV energy is not strong enough to operate it. The basic principle of storage- and converter-less energy harvesting is to provide the harvested energy directly to the computing node by exploiting a fine-grained dynamic power management (DPM).

As shown in Fig. 15, the MPP voltage of PV cell is maintained within a narrow range regardless of the solar irradiance. This means that the PV cell produces

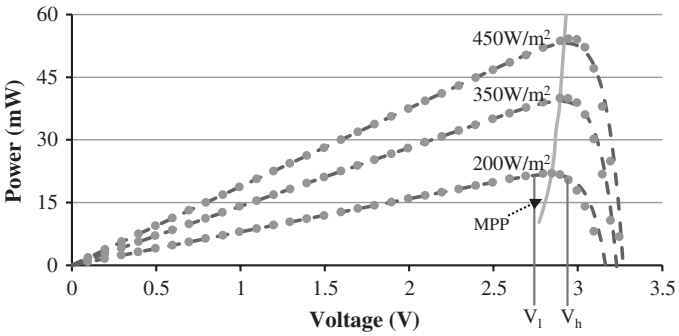

Fig. 15 Power-Voltage curve of a 4.5 × 5.5 cm^2 PV cell under different solar irradiance (Reproduced with permission from Wang et al. [24])

almost-constant voltage output, which is a main role of power converters, as long as we keep the track of the MPP current. Among the several ways to keep the track of the MPP current, fast enough DPM makes the PV cell keep the MPP as if the current of the load device is a DC current as long as the average current is the same to the MPP current. However, this may not be feasible if we do not carefully consider DPM overheads because fast DPMs may also bring nonnegligible energy and timing overheads during the state changes, which finally decreases the overall energy efficiency. So the proper control of the DPM frequency considering these overheads is necessary for maximizing the energy efficiency.

Storage-less operation does not directly affect the operation during a day even at very weak solar irradiance thanks to a very fine-grain DPM in a few hundreds microseconds. Although the load devices become unavailable after sunset, this may not be a serious problem in the applications where the operation is only required during the daytime.

4.2 Storage- and Converter-Less MPPT

Figure 16 illustrates the architecture of storage- and converter-less energy harvesting system proposed in [24]. Only single load switch with a DPM control logic is used in between the PV cell and load device. The DPM control logic continuously turns on and off the load switch depending on the level of the PV cell output voltage. Once the PV cell output voltage is higher than the upper threshold, V_h, the load device is turned on. Then, the PV cell output voltage decreases as the load devices are connected to the PV cell and the load current is higher than the MPP current. When the PV cell voltage becomes lower than the lower threshold, V_l, the MPP controller turns off the load switch and the PV cell output voltage recovers and goes back to V_h. This control policy maintains the PV cell output voltage within $[V_l, V_h]$.

The control process acts like a MPP tracking with the PV cell current steering as the load switch turns on and off faster than the cutoff frequency of the PV cell. This makes the PV energy harvesting system operational without power converters or an energy storage device while performing the MPPT.

The decoupling capacitor, C_{decoup} on the load side maintains power integrity of the load devices like normal devices. On the other hand, the bulk capacitor, C_{bulk}, connected in parallel with the PV cell extends the time constant of the PV cell so

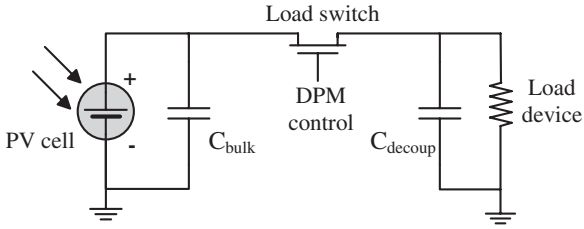

Fig. 16 Storage- and converter-less PV energy harvesting system

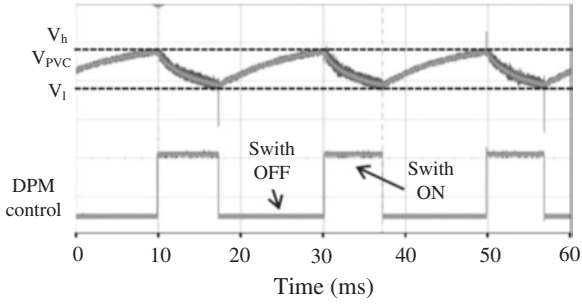

Fig. 17 Voltage changes depending on the DPM control (Reproduced with permission from Wang et al. [24])

that the PV cell's time constant may match with the feasible DPM period of the load devices. So the sizing of bulk capacitor plays an important role because it determines the DPM time granularity, voltage drop during charge sharing between the bulk capacitor and decoupling capacitor, and the time and energy overhead of the DPM scheme. The DPM period, T_{DPM}, can be estimated by

$$T_{\text{DPM}} \approx \left(\frac{V_h - V_l}{I_{\text{pvc,mpp}}} + \frac{V_{\text{mid}} - V_l}{I_{\text{on}} - I_{\text{pvc,mpp}}}\right) C_{\text{bulk}}. \tag{23}$$

where V_{mid} is the voltage after the charge sharing, $I_{\text{pvc,mpp}}$ is the output current at the MPPs of the PV cell, and I_{on} is the load current when the load device is on. V_{mid} is simply calculated from the size of C_{bulk} and C_{decoup}, V_h, and V_l.

So the larger bulk capacitor, the longer DPM period. If the bulk capacitor size is small, the PV cell output voltage decreases fast as the load current discharges the capacitor. If the bulk capacitor is large, the PV cell output voltage decrease slowly.

Figure 17 shows the voltage changes observed on the PV cell during the operation of the load device. Under the control of the DPM control signal, the PV cell output voltage swings within the MPP windows of $[V_h, V_l]$.

4.3 Overhead Analysis

Though storage- and converter-less energy harvesting architecture significantly improves the energy efficiency by providing the harvested energy from the PV cell directly to the load device, it also brings nonnegligible energy overheads which are not used for executing the task but used for changing the power states or preparing the task execution before/after power state changes.

For example, the task cannot be executed until all the components used in the load device are waked up from the power-off state even after the load switch is on. For guaranteeing the reliable device operation, the task also cannot be executed during the preparation of the power state changes from on state to off state just before turning off the load switch. This is a nonavoidable DPM overhead in the

storage- and converter-less architecture. If T_{DPM} is set too small, DPM overhead may not be negligible. As described in Eq. 23, the period of DPM is mainly controlled with the size of C_{bulk}, $I_{pvc,mpp}$, and configuration of threshold values.

Another overhead of the storage- and converter-less architecture is the energy loss during the charge sharing between C_{bulk} and C_{decoup} when the load switch is turned on. The amount of energy loss is controlled by varying the size of C_{bulk} and C_{decoup}. However adjusting the size of C_{decoup} is not desirable because it maintains power integrity of the load device. The larger bulk capacitor, the less energy loss during the charge sharing. This means that the energy loss is minimized if we set the size of C_{bulk} as large as possible. However, this is not a simple problem because the size of C_{bulk} is tightly coupled with the period of the DPM as well. In addition, the larger capacitor makes it harder to track MPP of PV cell, which directly affects the quality of MPPT, though it lowers energy loss during the charge sharing as well as DPM overhead. So adjusting the size of bulk capacitor considering the application characteristics is important for maximizing the energy efficiency of the energy harvesting systems.

5 Conclusions

Solar energy harvesting is one of the most promising renewable energy generation that directly produces electric energy from solar irradiance. Despite its range of advantages, partial shading and cell fault may significantly degrade the whole array performance. This chapter introduced a systematic design practice of a dynamically reconfigurable photovoltaic (PV) cell array. The design framework introduced in this chapter significantly enhances the state-of-the-art PV energy harvesting systems both in performance and cost thanks to the cross-layer optimization.

Acknowledgments This work is supported by the Center for Integrated Smart Sensors funded by the Ministry of Science, ICT & Future Planning as the Global Frontier Project.

References

1. Lee W, Kim Y, Wang Y, Chang N, Pedram M (2011) Versatile high-fidelity photovoltaic module emulation system. In: Proceedings of the ACM/IEEE international symposium on low power electronics and design (ISLPED)
2. Choi Y, Chang N, Kim T (2007) DC–DC converter-aware power management for low-power embedded systems. IEEE Trans Comput Aided Des Integr Circ Syst 26(8):1367–1381
3. Wang Y, Kim Y, Xie Q, Chang N, Pedram M (2011) Charge migration efficiency optimization in hybrid electrical energy storage (HEES) systems. In: Proceedings of the ACM/IEEE international symposium on low power electronics and design (ISLPED)
4. Hohm DP, Ropp ME (2003) Comparative study of maximum power point tracking algorithms. Prog Photovoltaics Res Appl 11(1):47–62

5. Esram T, Chapman P (2007) Comparison of photovoltaic array maximum power point tracking techniques. IEEE Trans Energ Convers 22(2):439–449
6. Subudhi B, Pradhan R (2013) A comparative study on maximum power point tracking techniques for photovoltaic power systems. IEEE Trans Sustain Energ 4(1):89–98
7. Kim Y, Wang Y, Chang N, Pedram M (2010) Maximum power transfer tracking for a photovoltaic-supercapacitor energy system. In: Proceedings of the ACM/IEEE international symposium on low power electronics and design (ISLPED), pp 307–312
8. Shao H, Tsui C-Y, Ki W-H (2009) The design of a micro power management system for applications using photovoltaic cells with the maximum output power control. IEEE Trans Very Large Scale Integr VLSI Syst 17(8):1138–1142
9. Shao H, Tsui C-Y, Ki W-H (2010) Maximizing the harvested energy for micro-power applications through efficient MPPT and PMU design. In: Proceedings of the Asia and South Pacific design automation conference (ASP-DAC), pp 75–80
10. Lu C, Park SP, Raghunathan V, Roy K (2010) Efficient power conversion for ultra low voltage micro scale energy transducers. In: Proceedings of the conference on design, automation and test in Europe (DATE), pp 1602–1607
11. Kim S, No K-S, Chou P (2011) Design and performance analysis of supercapacitor charging circuits for wireless sensor nodes. IEEE J Emerg Sel Top Circ Syst (JETCAS) 1(3):391–402
12. Kim S, Chou P (2012) Size and topology optimization for supercapacitor-based sub-watt energy harvesters. IEEE Trans Power Electron 28(4):2068–2080
13. Mungan ES, Lu C, Raghunathan V, Roy K (2012) Modeling, design and cross-layer optimization of polysilicon solar cell based micro-scale energy harvesting systems. In: Proceedings of the ACM/IEEE international symposium on low power electronics and design (ISLPED), pp 123–128
14. Sulaiman SA, Hussain H, Leh NN, Razali MSI (2011) Effects of dust on the performance of PV panels. World Acad Sci Eng Technol 58:588–593
15. Swaleh MS, Green MA (1982) Effect of shunt resistance and bypass diodes on the shadow tolerance of solar cell modules. Sol Cells 5:183–198
16. Patel H, Agarwal V (2008) Maximum power point tracking scheme for PV systems operating under partially shaded conditions. IEEE Trans Industr Electron 55:1689–1698
17. Nguyen TL, Low K (2010) A global maximum power point tracking scheme employing DIRECT search algorithm for photovoltaic systems. IEEE Trans Industr Electron 57(10):345634
18. Nguyen D, Lehman B (2008) An adaptive solar photovoltaic array using model-based reconfiguration algorithm. IEEE Trans Industr Electron 55(7):2644–2654
19. Velasco-Quesada G (2009) Electrical PV array reconfiguration strategy for energy extraction improvement in grid-connected PV systems. IEEE Trans Industr Electron 56(11):4319–4331
20. Chaaban MA (2010) Adaptive photovoltaic system. In: Proceedings of the annual conference on IEEE industrial electronics society (IECON)
21. Kim Y, Park S, Wang Y, Xie Q, Chang N, Poncino M, Pedram M (2011) Balanced reconfiguration of storage banks in a hybrid electrical energy storage system. In: Proceedings of the international conference on computer-aided design (ICCAD), pp 624–631
22. Wang Y, Lin X, Kim Y, Chang N, Pedram M (2014) Architecture and control algorithms for combating partial shading in photovoltaic systems. IEEE Trans Comput Aided Des 33(4):917–930
23. Lin X, Wang Y, Pedram M, Kim J, Chang N (2014) Designing fault-tolerant photovoltaic systems. IEEE Des Test 31(3):76–84
24. Wang C, Chang N, Kim Y, Park S, Liu Y, Lee HG, Luo R, Yang H (2014) Storage-less and converter-less maximum power point tracking of photovoltaic cells for a nonvolatile microprocessor. In: Proceedings of the Asia and South Pacific design automation conference (ASP-DAC), pp 379–384